



Engineered ascorbate peroxidase as a genetically-encoded reporter for electron microscopy

Citation

Martell, Jeffrey D., Thomas J. Deerinck, Yasemin Sancak, Thomas L. Poulos, Vamsi K. Mootha, Gina E. Sosinsky, Mark H. Ellisman, and Alice Y. Ting. 2013. "Engineered ascorbate peroxidase as a genetically-encoded reporter for electron microscopy." *Nature biotechnology* 30 (11): 1143-1148. doi:10.1038/nbt.2375. <http://dx.doi.org/10.1038/nbt.2375>.

Published Version

doi:10.1038/nbt.2375

Permanent link

<http://nrs.harvard.edu/urn-3:HUL.InstRepos:11717661>

Terms of Use

This article was downloaded from Harvard University's DASH repository, and is made available under the terms and conditions applicable to Other Posted Material, as set forth at <http://nrs.harvard.edu/urn-3:HUL.InstRepos:dash.current.terms-of-use#LAA>

Share Your Story

The Harvard community has made this article openly available.
Please share how this access benefits you. [Submit a story](#).

[Accessibility](#)

Published in final edited form as:

Nat Biotechnol. 2012 November ; 30(11): 1143–1148. doi:10.1038/nbt.2375.

Engineered ascorbate peroxidase as a genetically-encoded reporter for electron microscopy

Jeffrey D. Martell¹, Thomas J. Deerinck², Yasemin Sancak^{3,4}, Thomas L. Poulos⁵, Vamsi K. Mootha^{3,4}, Gina E. Sosinsky^{2,6}, Mark H. Ellisman^{2,6}, and Alice Y. Ting¹

¹Department of Chemistry, Massachusetts Institute of Technology, Cambridge, Massachusetts, USA

²National Center for Microscopy and Imaging Research, Center for Research on Biological Systems, University of California at San Diego, La Jolla, California, USA

³Departments of Systems Biology and Medicine, Harvard Medical School and Massachusetts General Hospital, Boston, Massachusetts, USA

⁴Broad Institute, Cambridge, Massachusetts, USA

⁵Departments of Molecular Biology and Biochemistry, Chemistry, and Pharmaceutical Sciences, University of California, Irvine, California, USA

⁶Department of Neurosciences, University of California at San Diego, La Jolla, California, USA

Abstract

Electron microscopy (EM) is the standard method for imaging cellular structures with nanometer resolution, but existing genetic tags are inactive in most cellular compartments¹ or require light and are difficult to use². Here we report the development of a simple and robust EM genetic tag, called “APEX,” that is active in all cellular compartments and does not require light. APEX is a monomeric 28 kDa peroxidase that withstands strong EM fixation to give excellent ultrastructural preservation. We demonstrate the utility of APEX for high-resolution EM imaging of a variety of mammalian organelles and specific proteins. We also fused APEX to the N- or C-terminus of the mitochondrial calcium uniporter (MCU), a newly identified channel whose topology is disputed^{3,4}. MCU-APEX and APEX-MCU give EM contrast exclusively in the mitochondrial matrix, suggesting that both the N- and C-termini of MCU face the matrix.

EM-level localization of proteins has been integral to elucidating many cellular processes. Antibody-based detection^{5–8}, the most common approach, requires either permeabilizing treatments, which degrade cellular ultrastructure^{9,10}, or ultracryosectioning of sucrose cryoprotected samples and immunostaining of each individual section¹¹. Genetically encoded tags do not require permeabilization, technically demanding ultracryosectioning, or staining of individual sections because they localize to the site of interest prior to fixation, but the existing genetic tags for EM have limitations. Horseradish peroxidase (HRP) is a

Correspondence should be addressed to A.Y.T. (ating@mit.edu).

AUTHORS' CONTRIBUTIONS STATEMENT

J.D.M. and A.Y.T. designed the research, analyzed the data, and wrote the paper. All authors edited the paper. M.H.E. and G.E.S. oversaw EM experiments and analyzed the results. T.L.P. provided guidance on peroxidases and peroxidase assays. J.D.M. and T.J.D. performed EM sample preparation and imaging. Y.S. and V.K.M. performed calcium uptake assays and prepared MCU stable cells. J.D.M. performed all other experiments.

COMPETING INTERESTS STATEMENT

Massachusetts Institute of Technology is seeking to file a patent application covering part of the information contained in this article.

sensitive¹² tag that catalyzes the H₂O₂-dependent polymerization of 3,3'-diaminobenzidine (DAB) into a localized precipitate that gives EM contrast after treatment with OsO₄^{13,14}. However, HRP is inactive when expressed in the mammalian cytosol¹, likely because its four structurally-essential disulfide bonds and two Ca²⁺ binding sites do not form in reducing and Ca²⁺-scarce environments. A genetically encoded tag called “miniSOG”² provides EM contrast in all cellular compartments *via* light-dependent generation of ¹O₂, which produces a DAB precipitate, but the requirement for light can be limiting when large or thick samples need to be stained for EM. ReAsH is another light-dependent tag, but its nonspecific labeling and the challenge of probe delivery into tissue limit its utility^{15,16}.

A re-engineered version of HRP with activity in the cytosol would overcome the limitations of existing methods¹⁷, but our attempts to remove its disulfide bonds abolished activity (data not shown). We instead searched for peroxidases that are naturally active in reducing environments. Ascorbate peroxidase (APX) is a class I cytosolic plant peroxidase that lacks disulfide bonds and calcium ions¹⁸. At 28 kDa, APX is also ~40% smaller than HRP. However, APX has not previously been tested in mammalian cells, and its natural substrate, ascorbate, has a structure that is very different from DAB (Fig. 1a). Furthermore, wild-type (wt) APX is a constitutive homodimer¹⁹, a problem since oligomeric tags can perturb a protein's natural localization and function²⁰.

We first tested expression and activity of wt APX, using immunostaining and Amplex UltraRed, a fluorogenic peroxidase substrate, in three cellular compartments: cytosol, mitochondrial matrix, and endoplasmic reticulum (ER). For comparison, we tested HRP in the same locations. APX expressed well and was active in all compartments, whereas genetically-targeted HRP was active only in the ER, as expected (Supplementary Fig. 1).

We proceeded to engineer a monomeric APX. Guided by the crystal structure¹⁸ and building upon an earlier mutagenesis study¹⁹, we individually mutated negatively charged or neutral residues at the dimer interface to Lys to introduce repulsive interactions (Fig. 1b). We also tested three mutants (K14D, K31S, and A233D) on the basis of sequence alignment to an isoform of maize APX that was reported to be monomeric²¹. Gel filtration chromatography (GFC) was used to assess oligomerization (Fig. 1c and Supplementary Fig. 2). Five mutants were significantly more monomeric than wt, but they all displayed weak dimerization, so we generated double and triple mutants using permutations of the five promising single mutations. APX K14D/E112K exhibited the most monomericity while still expressing well in *E. coli* and forming minimal high molecular weight aggregates.

We compared the oligomerization of APX K14D/E112K (=mAPX, for monomeric APX) to that of wt APX, miniSOG, and several fluorescent proteins (mApple, EYFP, and mEos2) across a range of concentrations (Fig. 1d). mAPX was not as monomeric as mApple, but it was comparable to EYFP and much more monomeric than both wt APX and mEos2²⁰. We fused both mAPX and wt APX to connexin43 (Cx43), a protein that is sensitive to oligomeric tags (Fig. 1e)^{20,22}. Whereas wt APX gave rise to abnormal retention inside cells, both Cx43-mAPX and Cx43-GFP-mAPX localized properly to gap junctions, indicating that despite its weak residual dimerization at high concentrations, mAPX does not disrupt Cx43 trafficking.

We compared the activity of wt APX and mAPX in mammalian cells. mAPX and wt APX were equally active *in vitro* and comparably active in some cellular contexts, such as the mitochondrial matrix, which houses the last step of heme biosynthesis (Fig. 2). However, when expressed throughout the cytosol *via* fusion to a nuclear export sequence (NES), mAPX was much less active than wt APX toward both DAB (Fig. 2) and Amplex UltraRed (Supplementary Fig. 3a–b). Culturing the cells with heme after transfection significantly

boosted the activity of mAPX-NES. We reasoned that the poor activity of mAPX-NES is likely due to less efficient heme incorporation in the cellular context, perhaps a result of decreased thermal stability associated with monomerization¹⁹.

In order to improve the performance of mAPX in mammalian cells, we engineered a monomeric APX with improved activity toward DAB in the hope that faster kinetics could compensate for diminished heme binding. We compared the substrate binding site of APX to that of HRP, which has faster kinetics and broader aromatic substrate tolerance²³. In order to make APX more HRP-like, we designed seven mutants of APX that incorporated mostly aromatic residues into the active site (Fig. 2a). We employed a colorimetric assay using guaiacol, a prototypical aromatic peroxidase substrate, to determine Michaelis-Menten kinetic parameters²⁴ (Fig. 2b and Supplementary Fig. 4). All of the mutations improved APX activity, with the most promising mutant showing >25-fold enhancement over wt APX in terms of k_{cat}/K_M . The most HRP-like mutant (W41F/G69F/D133A/T135F/K136F) was also the most active, validating our engineering approach.

To generate a monomeric APX with improved activity, we added the two mAPX mutations (K14D/E112K) to each of our activity-enhanced mutants. The monomerized versions of some activity-enhanced mutants performed poorly in several cellular contexts (Supplementary Fig. 5), but mAPX + W41F expressed well in *E. coli*, displayed minimal high molecular weight (MW) aggregation, and localized comparably to mAPX in cells. We therefore selected mAPX + W41F (K14D/E112K/W41F), which we call “APEX” (for Enhanced APX), as our optimized reporter for subsequent experiments. Importantly, APEX-NES gave markedly stronger staining in cells than mAPX-NES, using both DAB (Fig. 2c) and Amplex UltraRed (Supplementary Fig. 3) as substrates. APEX is as monomeric as mAPX *in vitro* (Fig. 1d) and behaves well as a fusion to Cx43, both alone and in tandem with GFP (Fig. 1e).

We proceeded to test the utility of APEX for EM imaging in mammalian cells. We first used APEX to stain two cellular compartments with distinct EM signatures: the mitochondrial matrix and the ER lumen. Mitochondria expressing APEX showed strong contrast and well-defined cristae structures relative to non-expressing mitochondria (Fig. 3a). When localized to the ER lumen, APEX provided dense staining throughout the ER tubular network (Fig. 3a). By comparison, the ER lumen of untransfected cells gave weak contrast.

We next performed EM imaging of APEX fused to three mammalian proteins: histone 2B (H2B), vimentin, and connexin43 (Cx43). APEX-H2B revealed detailed chromatin structures, both along the nuclear envelope and on the periphery of nucleoli (Fig. 3a). These features were not discernible in untransfected cells. APEX-H2B properly incorporated into chromatin throughout all stages of mitosis (Fig. 3a and Supplementary Fig. 6), demonstrating that the weak dimerization of APEX is non-perturbing in this context. Vimentin-APEX highlighted intermediate filaments throughout the cell, and subfilamentous repeating densities could be discerned (Fig. 3a), underscoring the excellent contrast and high resolution afforded by APEX. Cx43-GFP-APEX gave high-resolution images of gap junction plaques, revealed by both thin sections and electron tomography (Fig. 3a and Supplementary Movie 1). In some cases, gap junction plaques were closely apposed to tubular segments of ER membrane²⁵, but the DAB reaction product exhibited minimal spread even in the absence of membrane enclosure (Fig. 3a).

We used Cx43-GFP-APEX for correlated light microscopy (LM) and EM⁹ by imaging GFP fluorescence in fixed cells, followed by DAB deposition and EM processing (Fig. 3a). Similar constructs utilizing mCherry instead of GFP, in two different orientations, also

formed gap junctions and gave bright fluorescence and strong DAB staining (Supplementary Fig. 7).

Because APEX remains active after membrane-preserving cell fixation and generates a minimally-diffusive reaction product that does not cross membranes, we envisioned that APEX could be useful for determining the topology of membrane proteins. The mitochondrial calcium uniporter (MCU) is a recently-discovered channel protein responsible for calcium uptake into the mitochondrion^{3,4}. Each MCU subunit contains two transmembrane segments that span the inner mitochondrial membrane. Using a protease accessibility assay on purified mitochondria, Baughman et. al. proposed that both the N- and C-termini of MCU protrude into the mitochondrial matrix³. In contrast, DeStefani et. al. reported the opposite topology, with both the N- and C-termini facing the intermembrane space (IMS)⁴ (Fig. 3b). To resolve this discrepancy, we constructed N- and C-terminal fusions of APEX to MCU, performed DAB staining, and imaged the samples by EM. Consistent with the model of Baughman et. al., both constructs gave clear EM staining in the matrix, but not the IMS (Fig. 3c and Supplementary Fig. 8). Separate controls showed that APEX is active in the IMS (Supplementary Fig. 8).

Interestingly, the matrix stain was strongest for both constructs at sites where cristae were closely stacked (within ~25 nm). To investigate whether this localization is an artifact of APEX dimerization at high concentrations, we repeated the experiment using a tandem dimer of APX^{W41F} (description and characterization in Supplementary Fig. 9) as well as miniSOG in place of APEX. Identical EM staining patterns were obtained for all constructs (Supplementary Fig. 8), although we still cannot completely rule out artifactual dimerization because miniSOG, like APEX, shows weak oligomerization at concentrations above ~20 μ M (Fig. 1d). We also repeated the experiment with stable HeLa cells expressing MCU-APEX or APEX-MCU in place of endogenous MCU and obtained the same result (data not shown). In a functional assay for Ca²⁺ uptake, all fusions of MCU to APEX, tdAPX^{W41F}, and miniSOG performed comparably to MCU appended to a small Flag epitope tag (Fig. 3d), indicating that none of these tags perturb function. The MCU topology revealed by APEX EM imaging has implications for MCU interaction partners and regulatory proteins, as it is now clear that most of the soluble portions of the protein reside in the matrix, rather than the IMS.

In summary, we have developed APEX, an engineered variant of APX that is monomeric, can be targeted through transfection, and provides strong EM contrast in all cellular compartments thus far tested, including the cytosol, where HRP is inactive as a genetic tag. Although HRP-antibody conjugates provide sensitive EM staining of cytosolic targets, the permeablizing reagents required for immunostaining irreversibly damage cellular ultrastructure and allow the DAB reaction product to spread. In contrast, cells expressing APEX can be strongly fixed with 2% glutaraldehyde in the absence of detergent, and the reaction product is generated at 4 °C, enabling optimal preservation of ultrastructure and tight localization of the EM stain.

The APEX staining protocol is straightforward, requiring only the addition of DAB and H₂O₂. Photosensitizers such as miniSOG require light, which limits their utility in complex tissues and whole organisms, whereas APEX should be fully applicable for large-scale EM. Additionally, since APEX fusions provide a high-resolution 3-D reaction product, they are directly applicable to electron tomography (as demonstrated here), serial section analyses, and serial blockface scanning EM. MiniSOG has two advantages over APEX: it is smaller (12 kDa vs 28 kDa) and possesses intrinsic fluorescence, which facilitates correlated LM and EM. However, miniSOG's fluorescence is weak, and correlated imaging is best performed with miniSOG-fluorescent protein fusions²⁶. Here we show that APEX also

tolerates fusion to fluorescent proteins on either terminus, making correlated LM and EM straightforward. Because the APEX reaction conditions are orthogonal to miniSOG reaction conditions, it may be possible to utilize the two tags in combination to generate differentiable depositions of DAB for “two-color” EM.

Wt APX is a strong homodimer, but we have engineered APEX to be predominantly monomeric. APEX still shows residual dimerization at high concentrations, comparable to EYFP and miniSOG. Despite its weak dimerization, APEX behaves well as a fusion to numerous proteins that are sensitive to oligomerization. We did observe perturbation of ER structure when APEX was overexpressed on the ER membrane facing the cytosol (data not shown), similar to observations published for EGFP constructs²⁷. To avoid dimerization artifacts, we recommend expressing APEX at the minimum level required to obtain EM contrast.

One potential limitation of APEX is its requirement for heme. In many cell types and compartments, the endogenous heme available is sufficient to confer high APEX activity; all images in this work, except those in Figure 2c where indicated, were acquired without exogenous heme supplied. In heme-poor environments, however, such as the cytosol of some cell types, the activity of APEX toward DAB may be insufficient for EM, perhaps a result of diminished heme binding resulting from decreased stability¹⁹. In these cases, we recommend using APX^{W41F} instead of APEX if a dimeric tag can be tolerated, or supplementing the cell media with purified heme prior to fixation to increase the heme occupancy of APEX.

Beyond EM, APEX should have utility for a variety of other imaging and biotechnological applications, such as those for which HRP is currently used²⁸. For example, the activity of APEX toward numerous aromatic substrates (DAB, Amplex Red, and guaiacol are illustrated here) provides the opportunity not only for EM contrast, but also for colorimetric, fluorescent, and chemiluminescent readouts.

ONLINE METHODS

Cloning and mutagenesis

The pTRC99A bacterial expression vector encoding pea cytosolic APX with a His₆-tag appended to its N-terminus has been described previously³². Mutants of APX were generated using QuikChange mutagenesis (Stratagene) or overlap extension PCR³³. Some mutants were subcloned into the pET21a bacterial expression vector (EMD Chemicals) between the *Nde*I and *Xho*I restriction sites, which enabled higher protein yield than pTRC. Fusions of APX to mammalian proteins and localization signals were generated using standard restriction cloning methods. Supplementary Table 1 presents an overview of all mammalian expression constructs used in this study. For most of these mammalian expression constructs, the original pea APX gene was used. For some constructs, however, we used a pea APX gene with humanized codons, synthesized by GenScript. We avoided the use of HA epitope tags for immunofluorescence detection because the HA tag, being tyrosine rich, is oxidatively damaged by APX in the presence of H₂O₂.

Gel filtration chromatography

Purified APX, miniSOG, or fluorescent proteins were diluted to the desired concentrations using chilled (4 °C) phosphate buffered saline (PBS, 137 mM NaCl, 2.7 mM KCl, 10 mM Na₂HPO₄, 2.0 mM KH₂PO₄, pH 7.4) and then allowed to incubate at room temperature for 30 min to overnight. APX was not prone to aggregation on the timescale of hours at room temperature. Samples (100 µL) were run on a Waters HPLC system over a Superdex 75 10/300 column (GE Healthcare) that had been pre-equilibrated in PBS, pH 7.4. Samples

were run isocratically at room temperature in PBS at a flow rate of 0.5 mL/min. Elution of APX was monitored at 280 nm and 405 nm (heme absorbance). Empower software (Waters) was used for analysis of elution profiles. Apparent MWs were determined by referencing low molecular weight standards (GE) (Supplementary Fig. 2). For proteins that exhibited no significant change in apparent MW between 0.25 and 1 μ M, the apparent MW of the monomer was estimated to be equal to the apparent MW at 0.25 μ M. This estimation was applied for all proteins in Figure 1d except for wt APX, which was predominantly dimeric at 0.25 μ M. The apparent MW of the monomer for wt APX was assumed to be equal to the apparent MW of mAPX at 0.25 μ M.

Guaiacol activity assay

We attempted to establish an assay to monitor the APX-catalyzed polymerization of DAB *in vitro*, but could not determine the kinetic parameters for this complex process. Amplex UltraRed was also not utilized for kinetic measurements since the K_M of APX toward aromatic substrates is typically between 1 and 10 mM, and solutions of Amplex UltraRed cannot be economically prepared at these high concentrations. We utilized guaiacol as the substrate to measure peroxidase kinetics instead. Good activity toward guaiacol generally correlated well with robust polymerization of DAB *in vitro* (data not shown). Guaiacol assays were performed on a Nanodrop 2000c UV-vis spectrophotometer (Thermo Scientific) using its cuvette reader. HRP (Sigma) was prepared as a 10 μ M stock in PBS, flash frozen and stored at -80°C , and thawed immediately before use. Guaiacol peroxidase activity was measured according to the protocol of Lad et. al.²⁴ Briefly, guaiacol (Sigma) was diluted in room temperature PBS, pH 7.4, to concentrations ranging from 0.25 to 30 mM. Solutions were vortexed thoroughly to ensure the guaiacol was completely dissolved. H_2O_2 was added to a final concentration of 90 μ M, followed by addition of APX to a final concentration of 20 nM. For HRP, when 90 μ M H_2O_2 was used, all of the H_2O_2 was consumed so quickly that the initial rate of guaiacol turnover could not be determined on our spectrophotometer. Therefore, 10 mM H_2O_2 was used for HRP. Under these conditions, the initial rate of turnover was maintained for several seconds and could be readily determined. Oxidation to tetraguaiacol was monitored by absorbance at 470 nm ($\epsilon_{470} = 22 \times 10^3 \text{ M}^{-1}\text{cm}^{-1}$)²⁴. k_{cat} and K_M were calculated by nonlinear regression fitting to the Michaelis-Menten equation using OriginPro. All values are reported as the mean \pm standard deviation for 2–3 independent Michaelis-Menten fittings, with each fitting using at least 5 values of substrate concentration ranging between 0.25 and 30 mM.

Mammalian cell culture and transfection

HEK293T, HeLa, and COS-7 cells were cultured as a monolayer in Modified Eagle's Medium (MEM, Cellgro) supplemented with 10% fetal bovine serum (PAA Laboratories). Cells were maintained at 37°C under an atmosphere of 5% CO_2 . For EM imaging experiments, cells were grown on poly-d-lysine coated glass-bottom dishes (P35GC-0–14-C, MatTek Corp.). To improve the adherence of HEK293T cells, the dishes were also pretreated with 50 $\mu\text{g/mL}$ fibronectin (Millipore) for 1 hour at 37°C before cell plating. Cells were transfected at 60–90% confluence using Lipofectamine2000 (Life Technologies), typically with 0.7 μL Lipofectamine and 100 ng plasmid per 300,000 cells. Cells were labeled and/or fixed 18–24 h after transfection. For incubation of HEK293T cells with heme (Figure 2c), the media was supplemented with a heme-bovine serum albumin (BSA) complex (3 or 7 μM)³⁴ for 16–24 h, after which time the media was removed, cells were rinsed $1\times$ with non-heme-containing media, then processed for imaging. Note that all images, except those in Figure 2c where indicated, were acquired *without* exogenous heme supplied. APEX generally affords strong EM staining with no requirement for exogenous heme addition, so we recommend supplementing the media with heme only in cases where the DAB stain is not sufficiently strong for EM without heme addition.

DAB staining and preparation of cultured cells for EM

Transfected cells were fixed using room temperature 2% glutaraldehyde (Electron Microscopy Sciences) in buffer (100 mM sodium cacodylate with 2 mM CaCl_2 , pH 7.4), then quickly moved to ice. Cells were kept between 0 and 4 °C for all subsequent steps until resin infiltration. After 30–60 min, cells were rinsed 5×2 min in chilled buffer, then treated for 5 min in buffer containing 20 mM glycine to quench unreacted glutaraldehyde, followed by 5×2 min rinses in chilled buffer. A freshly-diluted solution of 0.5 mg/mL (1.4 mM) 3,3'-diaminobenzidine (DAB) tetrahydrochloride or the DAB free base (Sigma) dissolved in HCl were combined with 0.03% (v/v) (10 mM) H_2O_2 in chilled buffer, and the solution was added to cells for 1 to 15 min, depending on the sample. A summary of cell types and DAB reaction times is presented in Supplementary Table 2. The generation of reaction product could be monitored by transmitted light microscopy. To halt the reaction, the DAB solution was removed, and cells were rinsed 5×2 min with chilled buffer. Post-fixation staining was performed with 2% osmium tetroxide (Electron Microscopy Sciences) for 30 min in chilled buffer. Cells were rinsed 5×2 min in chilled distilled water, then placed in chilled 2% aqueous uranyl acetate (Electron Microscopy Sciences) overnight. The samples were then dehydrated in a cold graded ethanol series (20%, 50%, 70%, 90%, 100%, 100%) 2 min each, rinsed once in room temperature anhydrous ethanol to avoid condensation, and infiltrated in Durcupan ACM resin (Electron Microscopy Sciences) using 1:1 (v/v) anhydrous ethanol and resin for 30 min, then 100% resin 2×1 h, then into fresh resin and polymerized in a vacuum oven at 60 °C for 48 h.

Electron microscopy

DAB-stained areas of embedded cultured cells were identified by transmitted light, and the areas of interest were sawed out using a jeweler's saw and mounted on dummy acrylic blocks with cyanoacrylic adhesive (Krazy Glue, Elmer's Products). The coverslip was carefully removed, the block trimmed, and ultrathin (80 nm thick) sections were cut using an ultramicrotome (Leica Ultracut UTC6). Electron micrographs recorded using a JEOL 1200 TEM operating at 80 keV.

Amplex UltraRed labeling and immunostaining

Transfected cells on glass coverslips were moved to ice, then treated with a solution of 50 μM Amplex UltraRed (Molecular Probes) with 0.02% (6.7 mM) H_2O_2 in Dulbecco's phosphate-buffered saline (DPBS). The Amplex UltraRed solution was freshly diluted from a 10 mM stock in dimethyl sulfoxide. After 5 to 30 min, depending on the sample, the Amplex UltraRed solution was removed and replaced with DPBS. In some cases, cells were imaged live. Strong resorufin signal was present in cells expressing APX, although the signal was not tightly localized to the site of origin. Alternatively, Amplex UltraRed-stained cells were fixed using freshly depolymerized 4% formaldehyde (Electron Microscopy Sciences) in PBS for 30 min on ice, rinsed 5×2 min in chilled PBS, then treated with methanol for 5–10 min at -20 °C. Samples were blocked using 1% (v/v) bovine serum albumin (BSA, Fisher Scientific) in PBS at 4 °C for 30 min, then treated overnight at 4 °C with a 1:500 dilution of mouse-anti-Flag antibody (Agilent) or chicken-anti-c-myc antibody (Life Technologies) in PBS with 1% BSA. Cells were rinsed 4×5 min in PBS, then treated with a 1:750 dilution of AlexaFluor 488 goat anti-mouse IgG or AlexaFluor 568 goat anti-chicken IgG (Life Technologies) for 15 min at 4 °C. Cells were rinsed 4×5 min in PBS, then imaged by confocal microscopy. At this point, much of the resorufin had been washed away, but the remaining label was more closely localized to the site of origin.

Supplementary Material

Refer to Web version on PubMed Central for supplementary material.

Acknowledgments

We thank Amy Keating for use of her GFC system and Andrea Thor, Angela Cone, and Masako Terada for assistance with electron tomography. The IMS-APEX EM data were obtained by Hyun-Woo Rhee, Peng Zou, J.D.M., and Eliza Vasile (Microscopy and Imaging Core Facility, Koch Institute at MIT). Chaysith Uttamapinant (MIT) and Hunter Fraser (Stanford) provided helpful feedback on the manuscript. Funding was provided by NIH grants DP1 OD003961 (A.Y.T.), P41RR004050 (M.H.E.), P41GM103412 (M.H.E.), GM065937 (G.E.S.), GM072881 (G.E.S.), GM077465 (V.K.M), and GM42614 (T.L.P.). J.D.M. was supported by NSFGR and NDSEG fellowships.

References

1. Hopkins C, Gibson A, Stinchcombe J, Futter C. Chimeric molecules employing horseradish peroxidase as reporter enzyme for protein localization in the electron microscope. *Methods in enzymology*. 2000; 327:35. [PubMed: 11044972]
2. Shu X, et al. A Genetically Encoded Tag for Correlated Light and Electron Microscopy of Intact Cells, Tissues, and Organisms. *PLoS Biol*. 2011; 9:e1001041. [PubMed: 21483721]
3. Baughman JM, et al. Integrative genomics identifies MCU as an essential component of the mitochondrial calcium uniporter. *Nature*. 2011; 476:341–345. [PubMed: 21685886]
4. De Stefani D, Raffaello A, Teardo E, Szabo I, Rizzuto R. A forty-kilodalton protein of the inner membrane is the mitochondrial calcium uniporter. *Nature*. 2011; 476:336–340. [PubMed: 21685888]
5. De Mey J, Moeremans M, Geuens G, Nuydens R, De Brabander M. High resolution light and electron microscopic localization of tubulin with the IGS (immuno gold staining) method. *Cell Biology International Reports*. 1981; 5:889–899. [PubMed: 7028278]
6. Giepmans BNG, Deerinck TJ, Smarr BL, Jones YZ, Ellisman MH. Correlated light and electron microscopic imaging of multiple endogenous proteins using Quantum dots. *Nat Meth*. 2005; 2:743–749.
7. Henderson D, Weber K. Three-dimensional organization of microfilaments and microtubules in the cytoskeleton: Immunoperoxidase labelling and stereo-electron microscopy of detergent-extracted cells. *Experimental Cell Research*. 1979; 124:301–316. [PubMed: 389645]
8. Deerinck TJ, et al. Fluorescence photooxidation with eosin: a method for high resolution immunolocalization and in situ hybridization detection for light and electron microscopy. *The Journal of Cell Biology*. 1994; 126:901–910. [PubMed: 7519623]
9. Sosinsky, GE., et al. *Methods in Cell Biology*. Vol. 79. Academic Press; 2007. Markers for Correlated Light and Electron Microscopy; p. 575-591.
10. Schnell U, Dijk F, Sjollem KA, Giepmans BNG. Immunolabeling artifacts and the need for live-cell imaging. *Nat Meth*. 2012; 9:152–158.
11. Tokuyasu KT. Application of cryoultramicrotomy to immunocytochemistry. *Journal of Microscopy*. 1986; 143:139–149. [PubMed: 3531524]
12. Porstmann B, Porstmann T, Nugel E, Evers U. Which of the commonly used marker enzymes gives the best results in colorimetric and fluorimetric enzyme immunoassays: Horseradish peroxidase, alkaline phosphatase or [beta]-galactosidase? *Journal of Immunological Methods*. 1985; 79:27–37. [PubMed: 3923120]
13. Connolly CN, Futter CE, Gibson A, Hopkins CR, Cutler DF. Transport into and out of the Golgi complex studied by transfecting cells with cDNAs encoding horseradish peroxidase. *The Journal of Cell Biology*. 1994; 127:641–652. [PubMed: 7962049]
14. Li J, Wang Y, Chiu SL, Cline H. Membrane targeted horseradish peroxidase as a marker for correlative fluorescence and electron microscopy studies. *Frontiers in Neural Circuits*. 2010; 4
15. Gaietta G, et al. Multicolor and Electron Microscopic Imaging of Connexin Trafficking. *Science*. 2002; 296:503–507. [PubMed: 11964472]
16. Uttamapinant C, et al. A fluorophore ligase for site-specific protein labeling inside living cells. *Proceedings of the National Academy of Sciences*. 2010; 107:10914–10919.
17. Tsien R. Imaging imaging's future. *Nature reviews Molecular cell biology*. 2003;SS16–SS21. Supplement to volume 4.

18. Patterson WR, Poulos TL. Crystal structure of recombinant pea cytosolic ascorbate peroxidase. *Biochemistry*. 1995; 34:4331–4341. [PubMed: 7703247]
19. Mandelman D, Li H, Poulos TL, Schwarz FP. The role of quaternary interactions on the stability and activity of ascorbate peroxidase. *Protein Science*. 1998; 7:2089–2098. [PubMed: 9792095]
20. McKinney SA, Murphy CS, Hazelwood KL, Davidson MW, Looger LL. A bright and photostable photoconvertible fluorescent protein. *Nat Meth*. 2009; 6:131–133.
21. Koshiba T. Cytosolic Ascorbate Peroxidase in Seedlings and Leaves of Maize (*Zea mays*). *Plant and Cell Physiology*. 1993; 34:713–721.
22. Lauf U, Lopez P, Falk MM. Expression of fluorescently tagged connexins: a novel approach to rescue function of oligomeric DsRed-tagged proteins. *FEBS letters*. 2001; 498:11–15. [PubMed: 11389889]
23. Henriksen A, Smith AT, Gajhede M. The Structures of the Horseradish Peroxidase C-Ferulic Acid Complex and the Ternary Complex with Cyanide Suggest How Peroxidases Oxidize Small Phenolic Substrates. *Journal of Biological Chemistry*. 1999; 274:35005–35011. [PubMed: 10574977]
24. Lad L, Mewies M, Raven EL. Substrate Binding and Catalytic Mechanism in Ascorbate Peroxidase: Evidence for Two Ascorbate Binding Sites. *Biochemistry*. 2002; 41:13774–13781. [PubMed: 12427040]
25. Sosinsky GE, et al. Tetracysteine Genetic Tags Complexed with Biarsenical Ligands as a Tool for Investigating Gap Junction Structure and Dynamics. *Cell Communication and Adhesion*. 2003; 10:181–186. [PubMed: 14681013]
26. Qi YB, Garren EJ, Shu X, Tsien RY, Jin Y. Photo-inducible cell ablation in *Caenorhabditis elegans* using the genetically encoded singlet oxygen generating protein miniSOG. *Proceedings of the National Academy of Sciences*. 2012; 109:7499–7504.
27. Costantini LM, Fossati M, Francolini M, Snapp EL. Assessing the Tendency of Fluorescent Proteins to Oligomerize Under Physiologic Conditions. *Traffic*. 2012; 13:643–649. [PubMed: 22289035]
28. Ryan B, Carolan N, Ó'Fágáin C. Horseradish and soybean peroxidases: comparable tools for alternative niches? *Trends in Biotechnology*. 2006; 24:355–363. [PubMed: 16815578]
29. Berglund G, et al. The catalytic pathway of horseradish peroxidase at high resolution. *Nature*. 2002; 417:463–468. [PubMed: 12024218]
30. Sharp KH, Moody PCE, Brown KA, Raven EL. Crystal Structure of the Ascorbate Peroxidase Salicylhydroxamic Acid Complex. *Biochemistry*. 2004; 43:8644–8651. [PubMed: 15236572]
31. Kirmse, R.; Bouchet-Marquis, Cd; Page, C.; Hoenger, A.; Thomas, MIR. *Methods in Cell Biology*. Vol. 96. Academic Press; 2010. Chapter 23- Three-Dimensional Cryo-Electron Microscopy on Intermediate Filaments; p. 565-589.
32. Cheek J, Mandelman D, Poulos T, Dawson J. A study of the K⁺-site mutant of ascorbate peroxidase: mutations of protein residues on the proximal side of the heme cause changes in iron ligation on the distal side. *Journal of Biological Inorganic Chemistry*. 1999; 4:64–72. [PubMed: 10499104]
33. Ho SN, Hunt HD, Horton RM, Pullen JK, Pease LR. Site-directed mutagenesis by overlap extension using the polymerase chain reaction. *Gene*. 1989; 77:51–59. [PubMed: 2744487]
34. Richards MK, Marletta MA. Characterization of Neuronal Nitric Oxide Synthase and a C415H Mutant, Purified from a Baculovirus Overexpression System. *Biochemistry*. 1994; 33:14723–14732. [PubMed: 7527656]

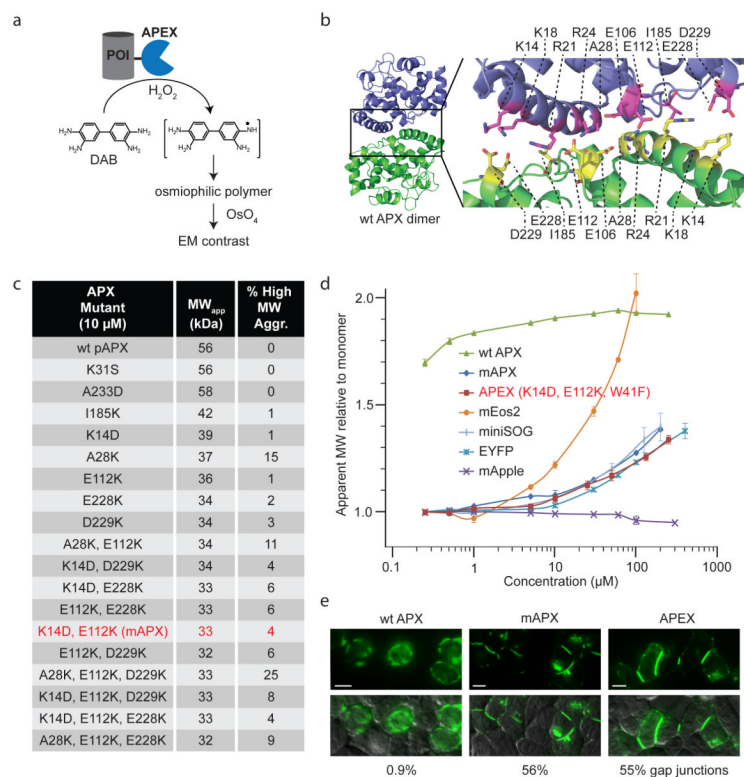


Figure 1. Electron microscopy reporter scheme and characterization of APEX oligomerization state

(A) The APEX reporter, a monomeric and activity-enhanced mutant of pea ascorbate peroxidase (APX), can be genetically fused to any cellular protein of interest (POI). After expression in live cells, the cells are fixed, and a solution of diaminobenzidine (DAB) is overlaid. Upon addition of H₂O₂, APEX, which retains activity in fixative, catalyzes the oxidative polymerization of DAB to generate a cross-linked precipitate. Subsequent staining of the DAB polymer with electron-dense OsO₄ generates EM contrast. (B) Mutations were introduced at the dimer interface of wild-type (wt) APX (from PDB ID 1APX¹⁸). (C) Mutants of APX were analyzed by gel filtration chromatography. The calculated molecular weight (MW) of wt APX is 28 kDa. As expected, wt APX runs as a dimer (apparent MW 56 kDa). Some mutants also formed higher molecular weight aggregates (MW_{app} >200 kDa), which may indicate instability. The K14D, E112K double mutant (mAPX, in red) was selected for further characterization. (D) Gel filtration analysis of mAPX, wt APX, and APEX at concentrations ranging from 250 nM to 250 μM. Dimerization of mAPX and APEX is not detected at <10 μM but some dimerization is seen at concentrations >50 μM. For comparison, similar analyses were performed under identical conditions for the fluorescent protein markers mEos2, EYFP, and mApple, as well as miniSOG². Error bars represent the standard deviation of 2–3 independent measurements. For data points with standard deviation values smaller than the height of the marker, no error bars are shown. (E) Imaging wt APX, mAPX, and APEX fusions to connexin43-GFP (C-terminal fusions) in live HEK293T cells. The top row shows GFP fluorescence (not normalized), and the bottom row shows GFP overlay onto the DIC image. Gap junctions could be easily detected for mAPX and APEX fusions (56 and 55% of contact sites between neighboring transfected cells contained GFP-labeled gap junctions, respectively), but not for the wt APX fusion (0.9%), which predominantly displayed fluorescence trapped in the secretory pathway. Scale bars, 10 μm.

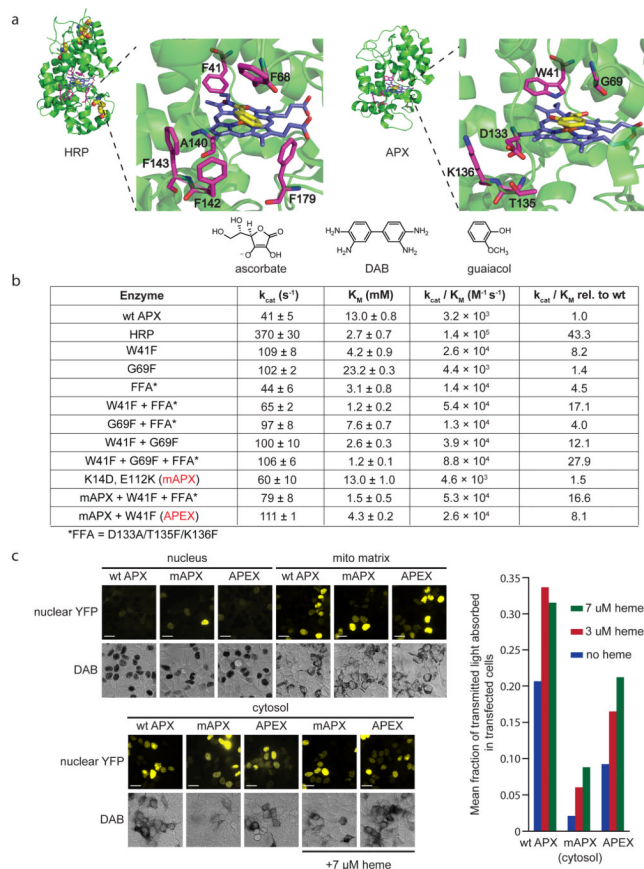
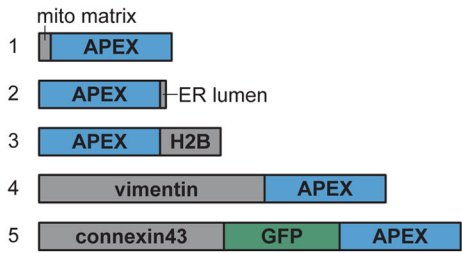
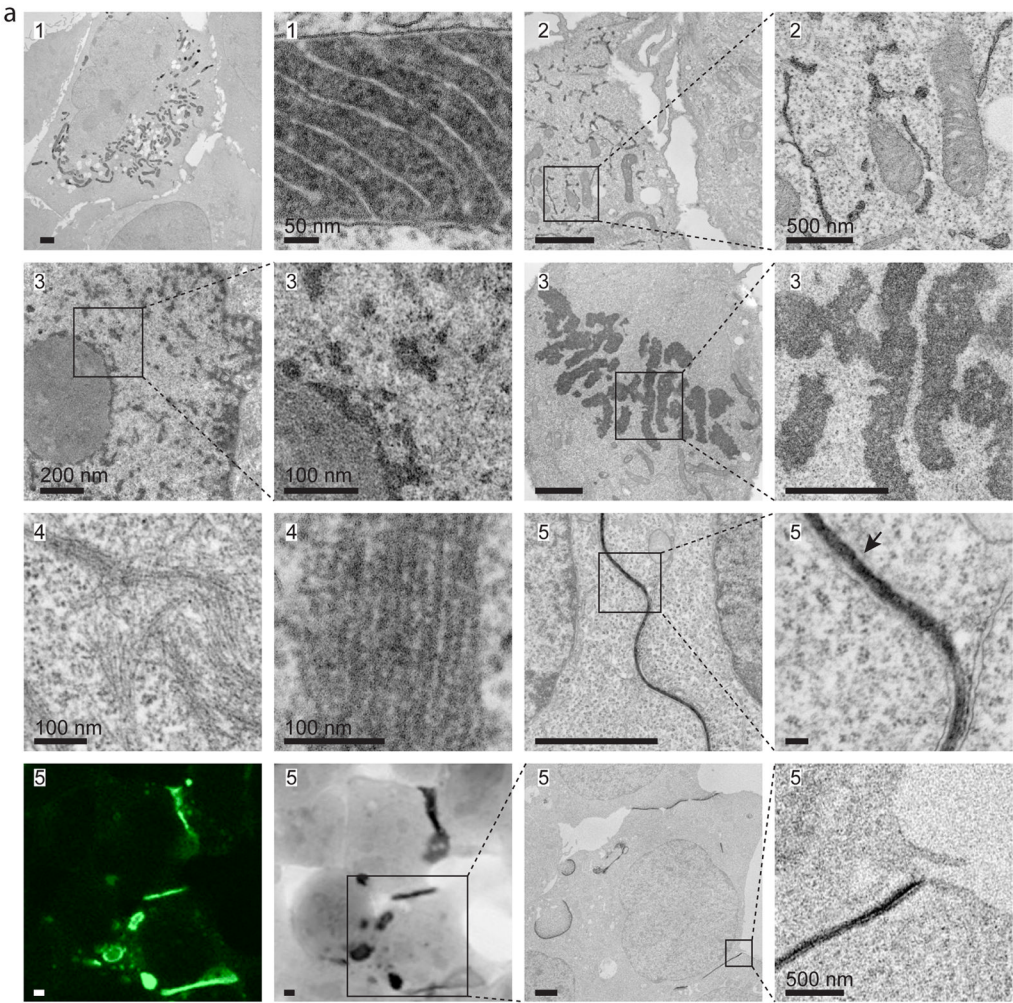


Figure 2. Active-site engineering to boost the activity of APEX

(A) Comparison between the active sites of wt HRP and wt APX (from PDB IDs 1H5A²⁹ and 1V0H³⁰, respectively). The heme cofactor is shown in blue. The co-crystallized substrate analogues (benzohydroxamic acid for HRP and salicylhydroxamic acid for APX) are shown in yellow. The HRP active site is lined with aromatic side chains, shown in purple, whereas the APX active site has only a single tryptophan at position 41. In the full HRP structure at left, the four disulfide bonds are rendered in space-filling yellow. Wt APX lacks disulfide bonds. Chemical structures of ascorbate (the natural substrate of APX), DAB (the desired substrate for EM applications), and guaiacol (a model aromatic substrate) are shown below. (B) Kinetic constants of APX mutants engineered to resemble HRP. k_{cat} and K_M values were measured using a spectrophotometric assay with guaiacol as substrate. (C) DAB polymerization activities of wt APX, mAPX, and APEX expressed in various cellular compartments. HEK293T cells were transfected with the indicated constructs, incubated with or without exogenous heme, fixed, reacted with DAB, then imaged. The top row shows fluorescence of co-transfected nuclear YFP marker. The bottom row shows the brightfield image. DAB polymer appears dark because it absorbs light throughout the visible spectrum. For nuclear-localized constructs, DAB stain blots out the nuclear YFP fluorescence, so bright YFP fluorescence indicates poor APX activity. Scale bars, 25 μm . The graph on the right quantifies the data for cytosolic constructs. For each condition, the mean fraction of transmitted light absorbed was calculated for >60 transfected cells, then averaged together. Wt APX is the most active toward DAB in cells, followed by APEX and then mAPX. For all three constructs, heme addition boosts activity.



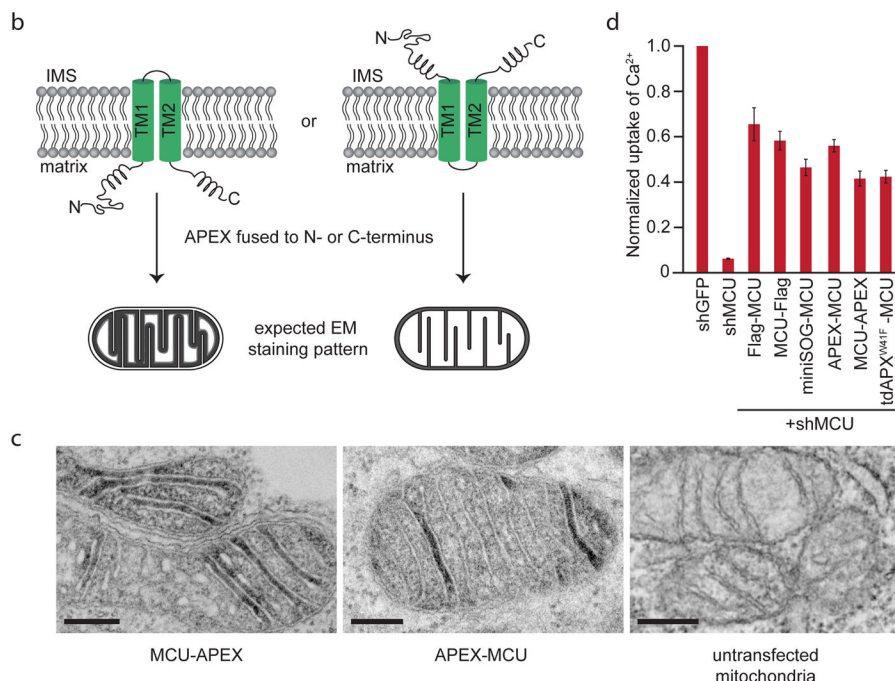


Figure 3. Electron microscopy of cellular proteins and organelles with APEX

(A) EM images of the genetic constructs shown at bottom. Additional EM images are shown in Supplementary Figure 6. (1) (*left*) Low magnification image of a COS-7 cell expressing APEX in the mitochondrial matrix. Compared to neighboring untransfected cells, the APEX-expressing mitochondria give much stronger contrast. (*right*) High magnification image of a single transfected mitochondrion. (2) COS-7 cell expressing endoplasmic reticulum-targeted APEX-KDEL. (3) COS-7 cells expressing APEX fusion to histone 2B. (*two left panels*) The zoom shows chromatin detail at the border of the nucleolus. (*two right panels*) COS-7 cell in metaphase of mitosis. Zoom shows chromosome detail. (4) Vimentin intermediate filaments in a COS-7 cell. APEX enables visualization of individual filaments, and a bead-like pattern with ~20 nm repeat spacing is apparent³¹. (5) (*top two panels*) Connexin gap junction between two transfected HEK293T cells. The zoom illustrates minimal spread of the DAB reaction product, even in the absence of membrane enclosure (arrow). (*bottom four panels*) Correlated light and electron microscopy of Cx43-GFP-APEX. Panels show (from left to right): fluorescence image prior to DAB stain, transmitted light image after DAB stain, low magnification EM image, and high magnification EM image. (B) Cartoon presenting the two topology models for the mitochondrial calcium uniporter (MCU) and the predicted EM staining patterns for each model when APEX is fused to either the N- or C-terminus of MCU. (C) EM images showing the DAB staining pattern for MCU-APEX (C-terminal fusion), APEX-MCU (N-terminal fusion), and untransfected mitochondria in COS-7 cells. Both MCU-APEX and APEX-MCU give clear staining in the mitochondrial matrix, while the intermembrane space (IMS) is light. In this experiment, the C32A mutant of APEX was used to eliminate the possibility of disulfide bond formation, but when APEX was used without the C32A mutation, identical results were obtained (data not shown). Additional fields of view for MCU fusion constructs are presented in Supplementary Figure 8. Scale bars, 200 nm. (D) MCU fusions to APEX are functional. Stable HeLa cells with endogenous MCU replaced by the recombinant MCU constructs shown were prepared by lentiviral infection followed by selection in geneticin. MCU-mediated calcium uptake into mitochondria was measured in these cells using Oregon Green Bapta 6F fluorescence. Error bars show the standard deviation from 4–6 independent

measurements. shMCU refers to control cells lacking MCU (endogenous or recombinant). shGFP refers to control cells expressing endogenous MCU.